ADVANCED OPTICAL MATERIALS
www.advopticalmat.de

Nanostructured Multilayer Coatings for Spatial Filtering

Lina Grineviciute, Ceren Babayigit, Darius Gailevičius, Martynas Peckus, Mirbek Turduev, Tomas Tolenis, Mikas Vengris, Hamza Kurt, and Kestutis Staliunas**

Spatial filtering is an important mechanism to improve the spatial quality of laser beams. Typically, a confocal arrangement of lenses with a diaphragm in the focal plane is used for intracavity spatial filtering. Such conventional filtering requires access to the far-field domain. In microlasers, however, conventional filtering is impossible due to the lack of space in microresonators to access the far-field. Therefore, a novel concept for more compact and efficient spatial filtering is necessary. In this study, a conceptually novel mechanism of spatial filtering in the near-field domain is proposed and demonstrated, by a nanostructured multilayer coating—a 2D photonic crystal structure with a periodic index modulation along the longitudinal and transverse directions to the beam propagation. The structure is built on a nanomodulated substrate, to provide the transverse periodicity. The physical vapor deposition is used to provide self-repeating modulation in the longitudinal direction. A 5 µm thick photonic multilayer structure composed of nanostructured multiple layers of alternating high- and low-index materials providing spatial filtering in the near-infrared frequencies with 2° low angle passband is experimentally demonstrated. The proposed photonic structure can be considered as an ideal component for intracavity spatial filtering in microlasers.

1. Introduction

Spatial filtering of light beams is an essential procedure in laser science and technology. Cleaning of the spatial distortions of the laser beams can be performed in postprocessing of the laser radiation to ensure the tight focusing or precise/controlled collimation of the light. However, even more important is the intracavity beam filtering inside of the laser resonators which enables the emission of maximally "clean" beam directly from the laser. In many kinds of lasers, the spatial distortions of the radiation are cleaned naturally due to the low aspect ratio of the system, when the longitudinal extent of the resonator is substantially larger than its transverse size, or due to resonators' curved mirrors with naturally occurring apertures. On the other hand, additional spatial filtering is sometimes performed by the intracavity spatial filter—a confocal lens arrangement with the aperture in the focal plane, which blocks higher-angle wave components (i.e., higher-order transverse modes) of the intracavity radiation. However, still for a large class of microlasers, such as semiconductor edge-emitting lasers, vertical-cavity surface-emitting lasers (VCSEL), microchip lasers, the intracavity spatial filtering is an unresolved issue. The natural beam cleaning mechanism is absent due to large aspect ratio of such microresonators, and the artificial filtering arrangement is impossible due to extremely small resonator dimensions (cavity length is in the order of millimeters, or in case of VCSEL—micrometers). A search for novel, efficient and convenient spatial filtering mechanisms, working in the near-field domain is crucial for the further development of such microlaser systems.

The spatial filtering in principle can be provided by photonic crystals (PhCs)—the structures with a periodically modulated refractive index on a wavelength scale, both longitudinally

L. Grineviciute, Dr. T. Tolenis
Center for Physical Sciences and Technology
Savanoriu Ave. 231, Vilnius LT-02300, Lithuania
E-mail: lina.grineviciute@ftmc.lt
C. Babayigit, Prof. H. Kurt
TOBB University of Economics and Technology
Söğütözü Str. 43, Ankara 06510, Turkey

The ORCID identification number(s) for the author(s) of this article can be found under https://doi.org/10.1002/adom.202001730.

DOI: 10.1002/adom.202001730

Dr. D. Gailevičius, Dr. M. Peckus, Prof. M. Vengris, Prof. K. Staliunas
Laser Research Center
Faculty of Physics
Vilnius University
Sauletekio Ave. 10, Vilnius LT-10223, Lithuania
E-mail: kestutis.staliunas@icrea.cat
Dr. D. Gailevičius
Femtika
Sauletekio Ave. 15, Vilnius LT-10224, Lithuania
Dr. M. Turduev
TED University
Ziya Gökalp Str. 48, Ankara 06420, Turkey
Prof. K. Staliunas
ICREA
Passeig Lluís Companys 23, Barcelona 08010, Spain
Prof. K. Staliunas
Departament de Fisica
Universitat Politècnica de Catalunya (UPC)
Rambla Sant Nebridi 22, Terrassa, Barcelona 08222, Spain

and transversely to the beam propagation direction.[1–4] Here, the filtering effect is based on the photonic bandgaps (BGs) of periodic media. Well known are the BGs in the frequency domain, which are due to the Bragg diffraction in layered (e.g., 1D index modulated) media, where the first BG occurs for the periods of modulation at around half-wavelength $\lambda/2$. Less evident is that also the angular BGs can occur in double-periodic (e.g., 2D index modulated) media, where the refraction index is modulated simultaneously in the longitudinal and transverse directions.[5]

The principal possibility of spatial filtering by PhCs already has been discussed,[1–4] but the experimental realization of the efficient spatial filters is still an unresolved issue. Volume refractive index modulation with the periods of around the $\lambda/2$ is technologically a great challenge. We note that the modulation must occur in 2D for 1D (cylindrical) spatial filtering, and in 3D for full (axisymmetric) spatial filtering. As the beams of several millimeter widths are to be cleaned in typical applications, the modulation must be perfectly uniform across the photonic structure over the ranges of millimeters. The transverse/longitudinal periods of the modulation must also be perfectly matched to provide the filtering on a given wavelength. Combining all these ingredients into one compact optical element is an unresolved challenge. Some attempts to fabricate spatial filters were made by direct laser writing in glasses,[6,7] and although they even were successfully integrated into microlasers,[8,9] they did not lead to spectacular improvement of the spatial structures of the radiation (the brightness increased 3 times in microchip lasers,[8] and 1.5 times in edge-emitting lasers[9]).

There are also alternative ideas on compact spatial filtering in metasurfaces, which can also provide angular sensitivity for plane waves reflecting/transmitting through the structure.[10] Various angular dispersion properties were demonstrated giving rise to incident-angle-selective meta-absorber, an angle-multiplexed meta-polarizer, an angle-multiplexed wavefront controller, and angle-multiplexed broadband metasurface sensor.[11,12] The aforementioned works are promising in perspective; however, they are still far from the technological applications in real photonic systems and high-power microlasers.

In this study, we propose and realize the spatial filtering effect based on the mechanism of the angular BGs in double-periodic photonic structures (see the schematic of the structure in **Figure 1**). Practically, the transverse periodicity results in a translation-invariant behavior, therefore such filters should be easy to align considering the fact that aligning optics precisely can be a very challenging task. From the technological viewpoint, the work combines lithographical methods to provide the seed of transverse modulation and the physical vapor deposition approach for longitudinal refractive index modulation. The transverse modulation was obtained by structuring the surface of the substrate by laser interference lithography, and the ion-beam sputtering process was used to conformally deposit multilayer coating on pre-microstructured substrates. There were also previous attempts to coat the microstructured substrates,[5,13] but no implementation has been presented. The thin films replicate the transverse seed modulation of the substrate and, as a result, the double-periodical modulation of the refractive index is obtained, which is a necessary ingredient for the PhC spatial filtering. The present article elaborates on the physical idea of filtering with its technological idea of fabrication. Moreover, the study presents a systematic search of the optimum geometry by simulations in finite-difference time-domain (FDTD) and plane-wave expansion (PWE) methods, an analytical approach of the design, fabrication using lithographic methods, multilayer coatings, and experimental measurements of spatial-angular transmission of the design. One of the main messages of the article is the first experimental demonstration of the functional 2D PhC spatial filter of several micrometer thicknesses for the near-infrared radiation.

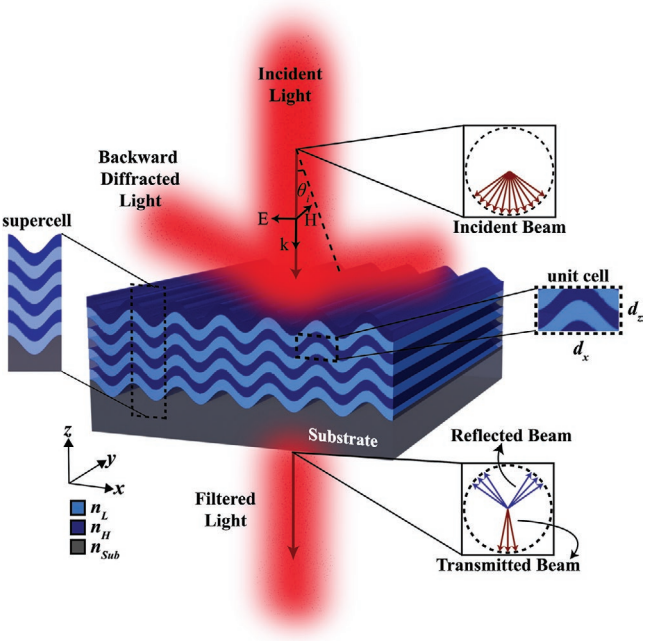

Figure 1. Photonic structure consisting of a self-replicating curved multilayer coating on a periodically modulated substrate. The insets show the elementary cell to calculate the photonic band diagrams, and the supercell used to calculate (angle, wavelength) diagrams of field transmission through the structure. The insets also illustrate the double-refraction based angle-selectivity of the transmission, providing the spatial filtering. Electric field is oriented for s-polarization case.

2. Design

The geometry of the photonic structure is schematically shown in Figure 1. The structure consists of alternating thin films with high and low refractive indices on a modulated substrate. The curved thin films replicate the surface modulation of the substrate, providing the refractive index modulation in both, the longitudinal (z-axis) and transverse (x-axis) directions. Note that the refraction from such a structure can be classified as the generalized Bragg one, since the refracted components propagate in a backward direction. The condition for the back-refraction is that the longitudinal component of the index modulation should have a periodicity of $\lambda/2 < d_z < \lambda$. This results in very compact dimensions of the filtering structure. For instance, 15 periods (30 layers) of modulation result in layered coatings of approximately 10 λ thickness, which, for the near IR, considering the refractive index of the material, is around 5 μm.

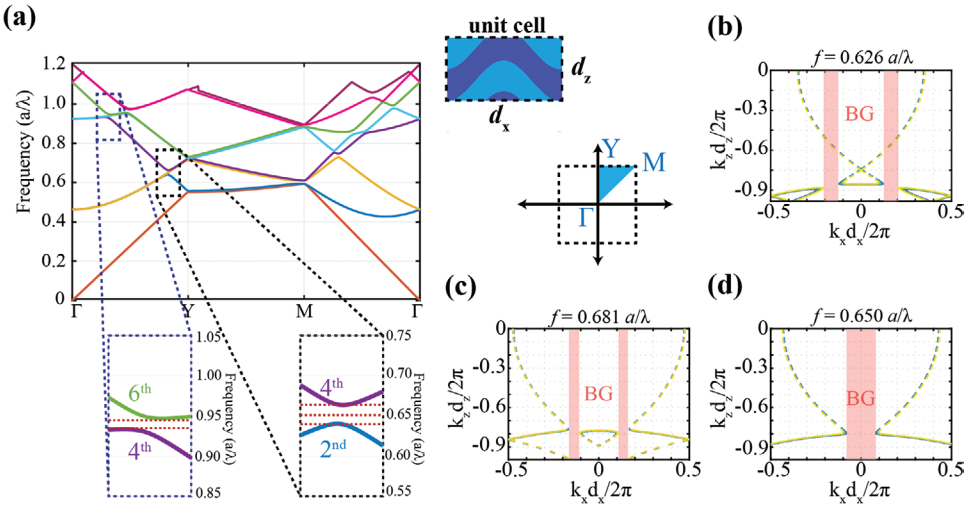

Figure 2. a) Band diagram of the (infinitely extended) periodic structure for the s-polarized electromagnetic field, with the regions of interest zoomed out (only second, and fourth bands indicated in the first, and fourth, and sixth bands in the second inset window). IFCs combined from second, third, and fourth bands, indicating high-angle-pass filtering at the middle of d) the first frequency BG, and low-angle-pass filtering below and above b,c) the first BG, respectively. Here, the Γ Y and M directions conventionally represent the points of high symmetries of 2D structures: Γ represents the center of the Brillouin zone, Y represents the center of a face along the light propagation direction, while M represents the corner point. These symmetry points are used to define the direction of the *k*-vectors. Parameters: transverse period $d_x = 600$ nm, longitudinal period $d_z = 301$ nm, modulation depth 150 nm, refractive indices $n_L = 1.99$ and $n_H = 2.24$. The wavelength is normalized to the lattice constant $a = d_x$.

This is a significant advantage of our filtering principle compared with the spatial filters in Laue configuration,[3,4,8,9] where the thickness of the spatial filter is of the order of 1 mm. Moreover, in Laue forward refraction configuration no "true" BGs are possible—just the quasi-BGs appear, as the refraction is directed predominantly in the forward direction. Furthermore, this thin arrangement of the filtering layers can support resonant wave-guiding modes if the coating has a higher refractive index than its surrounding media. Depending on the incidence angle and the wavelength of the incoming light, waveguiding modes can lead to enhanced/reduced transmission as a result of constructive/destructive interference and may improve the BG-based filtering effect.

The idea of the angular BGs filtering is first explored by the calculations of the band diagrams of the proposed structure by using the standard PWE method. To represent the band diagram of the structure in the reciprocal-space, we follow first the ΓY trajectory (i.e., along the beam propagation direction), then YM, and then back MΓ, see **Figure 2**a. Here, the BGs along the optical axis (ΓY-direction) are important for the filtering effect (see the inset dashed windows in the band-diagram, Figure 2a). In the middle of the axial BG, evidently, the axial components are blocked, which hints on the high-angle-pass spatial filtering effect. However, for the frequencies slightly below and above the axial BG the low-angle-pass filtering can be expected.

The scenario has been explored by calculating the isofrequency contours (IFCs) for the frequencies around the axial BG. We focus on the s-polarized electromagnetic field, where the electric field is directed parallel to the groves, in the main part of the article. The IFCs in Figure 2b–d are combined from the second, third, and fourth photonic bands, since the same frequency IFCs can be found in different bands. Indeed, for the frequencies inside the axial BG, the high-angle-pass filtering is obtained, see Figure 2d. For the frequencies slightly below and above the BG, the low-angle-pass filtering occurs as can be seen in Figure 2b,c, respectively. A complete collection of IFCs is presented in Suppl. 1 (Supporting Information). The filtering angular bandgaps actually consist of low angle pass areas, with the angles bounded from below by the isolines from second and fourth photonic bands, and the high angle pass area, with the angles bounded from above by isolines from third photonic bands at larger angles. In Figure 2b–d, the "relevant" isolines are indicated by the solid lines and "irrelevant: ones, which correspond to the "deaf" or "silent" modes, are shown by dashed lines. These "deaf" modes formally exist, but are not excited by the incident plane wave, since they are orthogonal, or almost orthogonal to the incident plane waves, and the incident radiation does not project into these modes.

Interestingly, the same scenario of low-high-low angle-pass filtering occurs also around the second frequency BG, although to a lesser extent, as indicated in Figure 2a and documented in Suppl. 1 (Supporting Information).

Next, we explore numerically the transmission of the plane waves through the photonic structure depending on their incidence angle and the wavelength. Due to the transverse periodicity, we used the supercell analysis of the field propagation by the FDTD method, with Bloch-periodic boundary condition on the lateral boundaries of the supercell.[14,15] Corresponding results are summarized in **Figure 3**a. Here, we present the results only for the s-polarized incident wave (electric field orientation is parallel to the fringe direction, i.e., parallel to the *y*-axis). The p-polarization gives qualitatively the same response, see Suppl. 2 (Supporting Information). Furthermore, analytically calculated angular-frequency bandgaps are presented and superimposed in Figure 3b (for detailed analytical derivations see Suppl. 3, Supporting Information). Also, the cross-sectional profiles of the transmittance maps are extracted for wavelengths of $\lambda = 1051$ and $\lambda = 972$ nm in Figure 3c,d, respectively.

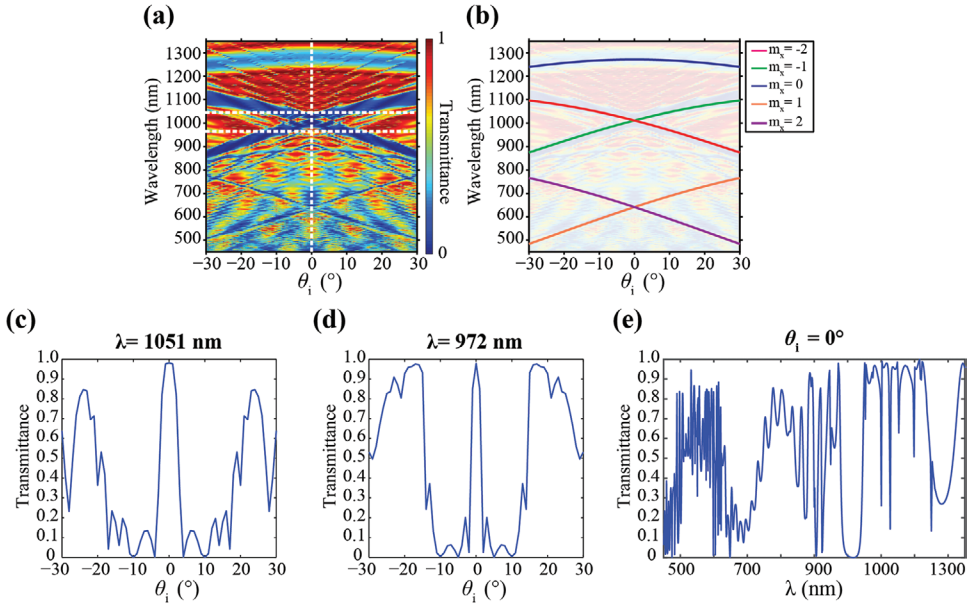

Figure 3. a) Map of transmission dependence on incidence angle and the wavelength extracted from the FDTD numerical calculations on a supercell. Two "crosses" of Bragg reflection lines are visible indicating the first and the second axial BG. Two dashed lines indicate cross-sectional transmission profiles of $\lambda = 1051$ nm and $\lambda = 972$ nm. b) Analytically calculated Bragg bandgap positions. Angular dependences of transmissions at different wavelengths of c) $\lambda = 1051$ nm and d) $\lambda = 972$ nm (horizontal cross-sections of the map) showing efficient spatial filtering at around the first filtering BG. e) Vertical cross-section at the incidence angle $\theta_i = 0°$ at the transmission map in (a). Here, the structural parameters are the same as in Figure 2 and the number of layers equal to $N = 33$.

Additionally, a vertical cross-sectional profile indicating the frequency BGs at the incidence angle $\theta_i = 0°$ is presented in Figure 3e. As can be seen from Figure 3c,d, almost perfect transmission occurs within small incidence angles and the waves at slightly larger angles are strongly suppressed in the transmitted light. Interestingly the second frequency BG also provides spatial filtering but with comparably lower efficiency, at around the wavelength of $\lambda = 620$ nm, however, a detailed study was not performed.

The overall filtering pattern (i.e., angular BGs positions presented in Figure 3a) corresponds well with the analytically calculated ones (Figure 3b), see the Suppl. 3 (Supporting Information). However, additionally, the transmission spectrum in the map was overlaid by the fringed structure. Vertical fringing is evidently related to the Fabry-Perot resonances of the coating structure, as the frequency separation between the fringes corresponds to the resonances of the structure of 5 µm geometrical thickness (10 µm optical thickness). The origin of the horizontal part of fringing is more sophisticated. We identify them as the resonances of the first-order diffracted modes trapped in the planar structure of a relatively high refraction index. The corresponding waveguided modes are calculated in Suppl. 4 (Supporting Information), resulting in a correct angular period of fringes. In addition to the main mechanism of the angle-selective refraction effect on a grating, the waveguiding effect can increase/decrease spatial filtering depending on the parameters (essentially on the thickness parameter of the coating). Further optimization of this additional effect can be used to improve the filtering performance of this type of spatial filter.

3. Fabrication and Characterization

The substrates with periodically transversally modulated surfaces were fabricated by laser interference lithography and nanoimprint technology. A chain of technological processes was applied to fabricate the samples. The fabrication process consists of the following steps: i) preparation of the master copy using the interference method in a photoresist ii) imprinting of the master structure on the substrate (using the UV imprint polymer); iii) physical vapor deposition on the modulated substrate to form the multilayered structure. The details are provided in the experimental section as well as in Suppl. 5 (Supporting Information).

The inner structure of the sample was characterized by using scanning electron microscope (SEM). In order to analyze the cross-sections, samples were cut by a laser beam and broken in the middle of the sample. Additionally, surface morphology was measured by atomic force microscope (AFM) before and after depositions of the coating to precisely determine the depths of the curved structure modulation, see **Figure 4**a.

Transmission maps for the fabricated sample were recorded by spectrophotometric measurements. Here, linearly polarized light was used for two perpendicular polarizations: s- and p-, where s-polarization is parallel to the grating lines on the sample. The angle between the main plane of the grating and the detector was varied from -30° to 30° by steps of 1°. The resulting transmission map is presented in Figure 4b.

The transmission maps correspond quantitatively to the ones obtained by numerical FDTD simulations. The main feature of the map—the crossings of the Bragg-reflection lines, is evident.

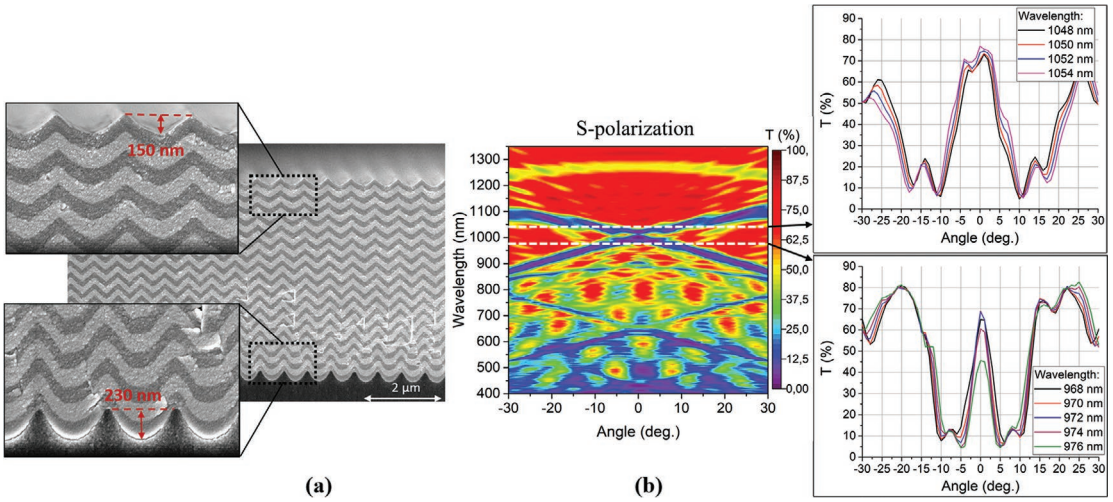

Figure 4. a) SEM images of the cross-section of the structure. b) Transmission map (transmission depending on the angle (horizontal axis) and wavelength (vertical axis)), together with cross-sections of the map (angular transmission curve) for characteristic wavelengths in the insets.

Also, the fringing is visible in the measured map. Similarly, to the numerical results, two crossings of the Bragg-reflection lines were observed, the main cross indicating the strong spatial filtering associated with the first BG and the weaker one associated with the second BG.

It should also be noted that SEM images of the cross-sections indicate a general tendency where the curving amplitude of the layers decreases with an increasing number of layers (see the inset cross-sections in Figure 4a). Typically, the modulation of the substrate with the amplitude of ≈220 nm decreases to the amplitude in the range of 110–150 nm at the top layer surface. The influence of the sweep of the modulation amplitude was also examined with the FDTD supercell analysis, and the obtained outcome showed that it did not essentially affect the results. The FDTD simulations with the modulation sweep lead to a weak deformation of the transmission maps without leading to essential modifications. The comparison is provided in Suppl. 6 (Supporting Information).

The main quantitative difference between numerical results and spectroscopic measurements of the fabricated structure is that the filtering lines in the latter case were less deep and more blurred. This can be attributed to the imperfections of fabricated structure—the corrugation of the substrate modulation on a range of around 10 μm and, subsequently, the corrugation of the whole structure. The influence of these large-scale imperfections is estimated in Suppl. 7 (Supporting Information).

4. Direct Proof of Spatial Filtering

Finally, the fabricated sample was illuminated by a cylindrically focused laser beam of a tunable picosecond laser (details of the laser device are provided in the experimental section). **Figure 5**a,b compares the far-field (angular) profiles of the incident probe beam and the resulting filtered beam for slightly different wavelengths. The narrowing of the angular spectra in the transmission is evident—angular divergence of the beam at FWHM is ≈2°. This is the main result of the article—specifically direct experimental proof for the spatial filtering effect by nanostructured multilayer coating.

For a more detailed analysis, a transmission map was reconstructed by dividing the measured angular intensity profile of the filtered beam by the reference (unfiltered) one. For comparison, we show the reconstructed transmission map in Figure 5c together with the one that obtained from spectrophotometric data in Figure 5d. Angular transmission spectra for two wavelengths of λ = 968 nm and λ = 972 nm are shown in Figure 5e,f for an additional comparison. The first case shows a transmission curve for a more bell-shaped profile with a higher transmission loss at the low angle values. On the other hand, the second case shows a lower loss case with a flat top resembling case. The detailed record of measurement data is provided in Suppl. 8 (Supporting Information). It is notable that the transmission through the structure did not exceed 80% whereas 100% would be more preferable for practical use at the angular intensity transmission bands. Here, both components of fabricated photonic structure: the substrate and the multilayer coating, are made of transparent, nonabsorbing materials for Vis-IR range. Since optical losses arise from the scattering and reflections, it can be controlled by using an optimized design of multilayer coating (including antireflective properties).

5. Discussion

The main message of the article is the demonstration of pronounced functional spatial filtering by thin nanostructured multilayer coating and with detailed numerical, analytical and experimental data, we are able to demonstrate such filtering of light. However, some imperfections still prevent the filter from technical applications, which should be discussed below and could be tackled in future work.

One issue is the broadening of the filtering lines due to the technical artifacts—the corrugation of the substrate on a large scale, and of the structure itself. With the current technology of the substrate fabrication, this limits the half-width of the filtering

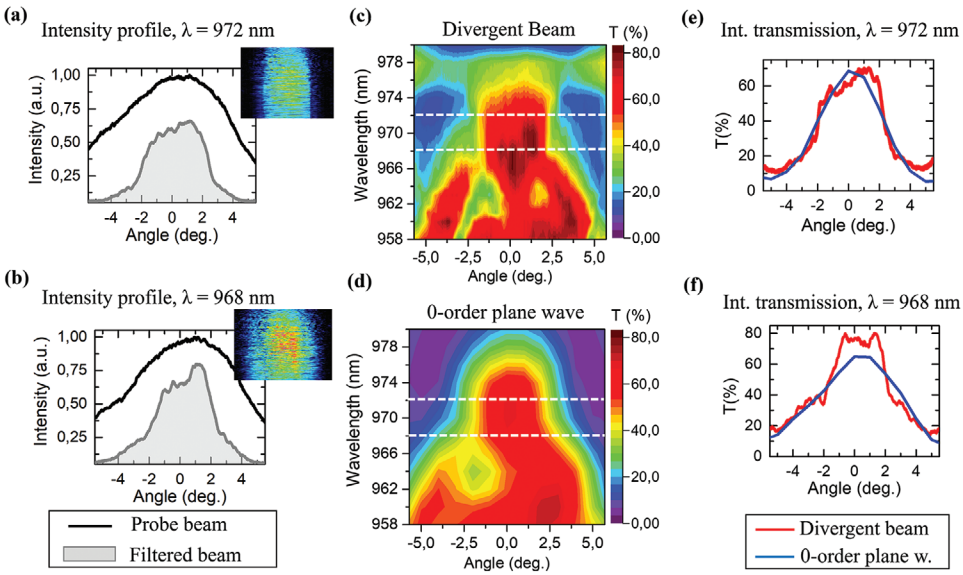

Figure 5. Experimental data for spatial filtering of a divergent probe beam. a,b) Transmission of a reference beam and filtered beam evidencing 1D (cylindrical) spatial filtering for two different wavelengths. Insets show the 2D intensity profiles of the filtered beam, registered on a CMOS camera. c) The corresponding transmission map, where the sample was illuminated with a divergent probe beam. Wavelengths of interest are marked with dotted lines. d)The zoomed-in range from Figure 4b corresponding to a zero-order plane wave transmission spectral-angular map. e,f) The intensity transmission profiles for wavelengths 972 and 968 nm for both measurement methods.

line approximately to 2°. As numerical simulations show, the removal of corrugation would allow reducing the half-width of filtering lines to approximately 1° for the current configuration.

The other issue is that the demonstrated filtering is a cylindrical one. The extension to 2D is, however, straightforward and consists in a change of the substrate modulation geometry (to square, hexagonal, concentric, etc.). The filtering geometry depends solely on the substrate, as the subsequent coating of layers in the vertical direction is independent of the geometry of the modulation of the substrate.

Hence, the fabricated multilayer structure (1D filtering, 2θ half-angle) could be well applied for broad area semiconductor edge emission lasers, where the reduction of the beam divergence from typical 5°–10°, to desired 1°–2° would be very profitable. The filters for the other relevant systems can require different angular widths of the transmission. To reduce the width (to obtain narrower angular transmission lines) generally the index contrast of deposited layers should be decreased, and the number of layers is increased.

6. Experimental Section

A variety of methods were used to achieve the main result—the demonstration of spatial filtering.

Design of the structure is based on numerical simulations using standard methods: plane wave expansion in a perfectly periodic structure to calculate the frequency isolines; FDTD simulations on a supercell to calculate the (angle, wavelength) transmission maps. Both are well-established methods.[15,16] For the proof of the spatial filtering, the full FDTD simulations on a complete structure were performed, which is also a well-established method.

Fabrication: The laser interference lithography, employing the third harmonics of Nd:YAG laser radiation, was used to form the master grating. Subsequently, the master was used in a typical soft nanoimprint lithography process,[17,18] where an intermediate soft polydimethylsiloxane imprint was taken from it and used for UV cured polymer (OrmoComp, $n_{ref} = 1.52$) copies production. The resulting samples with sinusoidally modulated surfaces (600 nm transverse period and 220 nm modulation depth) were used as the substrate for multilayer coating. The coating consists of alternating high and low refractive index thin films, deposited by the Ion Beam Sputtering method. Specifically, hafnia and niobia materials were used with refractive indices $n_L = 1.99$ and high $n_H = 2.24$, respectively. The multilayer structure consists of 33 layers, whose optical thicknesses were equal for both the high and low refractive index layers—317 nm ($d_z = 301$ nm with the geometric thicknesses—141.8 and 159.2 nm, respectively). More technical details are provided in Suppl. 5 (Supporting Information).

Characterization was performed by the AFM analysis of the surface's morphology of the substrate and of the upper layer of the fabricated structure. SEM was used to explore the cross-section of the fabricated structure. Finally, the spectroscopical measurements of the transmission were performed in order to build the (angle, wavelength) transmission maps.

Demonstration of spatial filtering by recording the far-field profiles of the transmitted beam from a tunable picosecond laser source, tuned in the wavelength range of 958 nm $\leq \lambda \leq$ 980 nm using a monochromator with a spectral bandwidth of approximately $\Delta\lambda \approx 1$ nm. Focusing provides the angular divergence of the beam of ≈9.7° at FWHM (full width at half maximum) in the horizontal direction. The resulting filtered beam was registered with a CMOS beam profiler camera while imaging the beam directly onto the sensor.

Supporting Information

Supporting Information is available from the Wiley Online Library or from the author.

Acknowledgements

This project has received funding from European Social Fund (project No 09.3.3- LMT-K712-17- 0016) under grant agreement with the Research Council

of Lithuania (LMTLT), D.G. and M.P. acknowledge the financial support from "FOKRILAS" (Project No. P-MIP-17-190) from Research Council of Lithuania. Authors are grateful to Dr. Algirdas Selskis from State research institute Center for Physical Sciences and Technology for SEM measurements.

Conflict of Interest

The authors declare no conflict of interest.

Author Contributions

K.S. supervised the project and provided theoretical analysis. C.B., M.T., H.K. performed the simulations. L.G. and D.G. fabricated modulated substrates, L.G., T.T., and D.G. designed and carried out the experiments and measurements. M.P. and M.V. performed measurements with a divergent laser beam. All authors participated in discussions and reviewed the manuscript.

Data Availability Statement

The data that supports the findings of this study are available in the supplementary material of this article.

Keywords

metamaterials, microlasers, photonic crystals, physical vapor deposition, spatial filtering

Received: October 8, 2020
Revised: February 17, 2021
Published online: March 16, 2021

[1] K. Staliunas, V. J. Sánchez-Morcillo, *Phys. Rev. A* **2009**, *79*, 053807.
[2] E. Colak, A. O. Cakmak, A. E. Serebryannikov, E. Ozbay, *J. Appl. Phys.* **2010**, *108*, 113106.
[3] L. Maigyte, T. Gertus, M. Peckus, J. Trull, C. Cojocaru, V. Sirutkaitis, K. Staliunas, *Phys. Rev. A* **2010**, *82*, 043819.
[4] V. Purlys, L. Maigyte, D. Gailevičius, M. Peckus, M. Malinauskas, K. Staliunas, *Phys. Rev. A* **2013**, *87*, 033805.
[5] L. Grinevičiūtė, C. Babayigit, D. Gailevičius, E. Bor, M. Turduev, V. Purlys, T. Tolenis, H. Kurt, K. Staliunas, *Appl. Surf. Sci.* **2019**, *481*, 353.
[6] L. Maigyte, K. Staliunas, *Appl. Phys. Rev.* **2015**, *2*, 011102.
[7] D. Gailevičius, V. Purlys, K. Staliunas, *Opt. Lett.* **2019**, *44*, 4969.
[8] D. Gailevicius, V. Koliadenko, V. Purlys, M. Peckus, V. Taranenko, K. Staliunas, *Sci. Rep.* **2016**, *6*, 34173..
[9] S. Gawali, D. Gailevičius, G. Garre-Werner, V. Purlys, C. Cojocaru, J. Trull, J. Montiel-Ponsoda, K. Staliunas, *Appl. Phys. Lett.* **2019**, *115*, 141104.
[10] J. Cheng, S. Inampudi, H. Mosallaei, *Sci. Rep.* **2017**, *7*, 12228.
[11] N. Born, I. Al-Naib, C. Jansen, R. Singh, J. V. Moloney, M. Scheller, M. Koch, *Adv. Opt. Mater.* **2015**, *3*, 642.
[12] A. Leitis, A. Tittl, M. Liu, B. H. Lee, M. B. Gu, Y. S. Kivsha, H. Altug, *Sci. Adv.* **2019**, *5*, eaaw2871.
[13] J. B. Oliver, T. J. Kessler, B. Charles, C. Smith, presented at *SVC Techcon*, Chicago, IL, May 2014.
[14] A. Taflove, S. C. Hagness, *Computational Electrodynamics: The Finite-Difference Time-Domain Method*, Artech House, Norwood, MA **2005**.
[15] B. Liang, M. Bai, H. Ma, N. Ou, J. Miao, *IEEE Trans. Antennas Propag.* **2014**, *62*, 354.
[16] S. G. Johnson, J. Joannopoulos, *Opt. Express* **2001**, *8*, 173.
[17] T. Tamulevičius, S. Tamulevičius, M. Andrulevičius, E. Griškonis, L. Puodžiukynas, G. Janušas, A. Guobienė, *Exp. Tech.* **2008**, *32*, 23.
[18] Y. Xia, G. M. Whitesides, *Annu. Rev. Mater. Sci.* **1998**, *28*, 153.